minerals

MDPI

Article

Phase Evolution from Volborthite, $Cu_3(V_2O_7)(OH)_2 \cdot 2H_2O$, upon Heat Treatment

Rezeda M. Ismagilova [1,2], Elena S. Zhitova [1,*], Sergey V. Krivovichev [2,3], Anastasia V. Sergeeva [1], Anton A. Nuzhdaev [1], Leonid P. Anikin [1], Mariya G. Krzhizhanovskaya [2], Maria A. Nazarova [1], Anastasia N. Kupchinenko [1], Andrey A. Zolotarev [2], Anton V. Kutyrev [1], Daria S. Bukhanova [1], Ruslan A. Kuznetsov [1] and Dmitry A. Khanin [4]

1 Institute of Volcanology and Seismology, Russian Academy of Sciences, Bulvar Piypa 9, 683006 Petropavlovsk-Kamchatsky, Russia; rezeda.m.ismagilova@gmail.com (R.M.I.); anastavalers@gmail.com (A.V.S.); nuzhdaev@gmail.com (A.A.N.); alp@kscnet.ru (L.P.A.); nazarovamar@mail.ru (M.A.N.); kupchasta@yandex.ru (A.N.K.); anton.v.kutyrev@gmail.com (A.V.K.); dasha-snejinka@yandex.ru (D.S.B.); ruslanalexeevich@yandex.ru (R.A.K.)

2 Institute of Earth Sciences, St Petersburg State University, Universitetskaya Nab. 7/9, 199034 St. Petersburg, Russia; skrivovi@mail.ru (S.V.K.); krzhizhanovskaya@mail.ru (M.G.K.); aazolotarev@gmail.com (A.A.Z.)

3 Nanomaterials Research Centre, Kola Science Centre, Russian Academy of Sciences, Fersman Street 14, 184209 Apatity, Russia

4 Institute of Experimental Mineralogy, Russian Academy of Sciences, Academica Osypyana ul., 4, 142432 Chernogolovka, Russia; mamontenok49@yandex.ru

* Correspondence: zhitova_es@mail.ru

Citation: Ismagilova, R.M.; Zhitova, E.S.; Krivovichev, S.V.; Sergeeva, A.V.; Nuzhdaev, A.A.; Anikin, L.P.; Krzhizhanovskaya, M.G.; Nazarova, M.A.; Kupchinenko, A.N.; Zolotarev, A.A.; et al. Phase Evolution from Volborthite, $Cu_3(V_2O_7)(OH)_2 \cdot 2H_2O$, upon Heat Treatment. *Minerals* **2021**, *11*, 1312. https://doi.org/10.3390/min11121312

Academic Editors: Tamara Đorđević, Natalia V. Zubkova and Igor Djerdj

Received: 19 October 2021
Accepted: 22 November 2021
Published: 24 November 2021

Abstract: In the experiments on volborthite in situ and ex situ heating, analogues of all known natural anhydrous copper vanadates have been obtained: ziesite, pseudolyonsite, mcbirneyite, fingerite, stoiberite and blossite, with the exception of borisenkoite, which requires the presence of As in the V site. The evolution of Cu-V minerals during in situ heating is as follows: volborthite $Cu_3(V_2O_7)(OH)_2 \cdot 2H_2O$ (30–230 °C) → X-ray amorphous phase (230–290 °C) → ziesite β-$Cu_2(V_2O_7)$ (290–430 °C) → ziesite + pseudolyonsite α-$Cu_3(VO_4)_2$ + mcbirneyite β-$Cu_3(VO_4)_2$ (430–510 °C) → mcbirneyite (510–750 °C). This trend of mineral evolution agrees with the thermal analytical data. These phases also dominate in all experiments with an ex situ annealing. However, the phase compositions of the samples annealed ex situ are more complex: fingerite $Cu_{11}(VO_4)_6O_2$ occurs in the samples annealed at ~250 and ~480 °C and quickly or slowly cooled to room temperature, and in the sample annealed at ~850 °C with fast cooling. At the same time, blossite and stoiberite have been found in the samples annealed at ~480–780 and ~780–850 °C, respectively, and slowly cooled to room temperature. There is a trend of decreasing crystal structure complexity in the raw phases obtained by the in situ heating with the increasing temperature: volborthite → ziesite → mcbirneyite (except of pseudolyonsite). Another tendency is that the longer the sample is cooled, the more complex the crystal structure that is formed, with the exception of blossite, most probably because blossite and ziesite are polymorphs with identical crystal structure complexities. The high complexity of fingerite and stoiberite, as well as their distinction by Cu:V ratio, may explain the uncertain conditions of their formation.

Keywords: volborthite; copper vanadate; high temperature; thermal analysis; ziesite; mcbirneyite; pseudolyonsite; blossite; stoiberite; fingerite

1. Introduction

Volborthite, $Cu_3(V_2O_7)(OH)_2 \cdot 2H_2O$, is commonly considered as a mineral formed in the oxidation zones of Cu-V deposits [1,2] (Table 1). Apart from volborthite, two other OH- or H_2O-containing copper vanadates are known: molinelloite, $Cu(H_2O)(OH)V^{4+}O(V^{5+}O_4)$ [3], and turanite, $Cu_5(VO_4)_2(OH)_4$ [4]; both are considered as hypergene minerals. Recently,

volborthite has been described in volcanically related environments: at the Alaid volcano (Kuril Islands, Russia) [5], Vesuvius Volcano (Southern Italy) [6] and in paleofumaroles of the Mountain 1004 (Tolbachik, Kamchatka, Russia) [7]. For the volborthite from Alaid volcano and Mountain 1004, it is assumed that, in these localities, the mineral was formed as a result of hypergene processes, altering the primary fumarolic Cu and V minerals. The list of potential fumarolic minerals that could serve as a source of Cu and V is long, however, it is noteworthy that all known natural anhydrous copper vanadates come from fumarolic environments (Table 1). To date, seven copper vanadates have been found in nature: blossite [8] and ziesite [9], which are orthorhombic and monoclinic polymorphs of $Cu_2(V_2O_7)$, respectively; fingerite [10], $Cu_{11}(VO_4)_6O_2$; mcbirneyite [11] and pseudolyonsite [12], which are triclinic and monoclinic polymorphs of $Cu_3(VO_4)_2$, respectively; borisenkoite [13], $Cu_3[(V,As)O_4]_2$; stoiberite, $Cu_5(VO_4)_2O_2$ [14]. These anhydrous copper vanadates are endemic or found in a couple of localities worldwide. Blossite, ziesite, fingerite, mcbirneyite and stoiberite have been found in fumaroles at the Izalco volcano (Sonsonate Department, El Salvador), while pseudolyonsite and borisenkoite come from the fumaroles of Tolbachik volcano (Kamchatka, Russia).

Table 1. Summary of known copper vanadates found in nature.

Mineral	Symmetry	Chemical Formula	Geological Setting	References
OH/H_2O-Containing Copper Vanadates				
Volborthite	Monoclinic	$Cu_3(V_2O_7)(OH)_2 \cdot 2H_2O$	Hypergene, paleofumarolic(?) or hypergene after fumarolic minerals	[1,2,5–7]
Molinelloite	Triclinic	$Cu(H_2O)(OH)V^{4+}O(V^{5+}O_4)$	Hypergene	[3]
Turanite	Triclinic	$Cu_5(VO_4)_2(OH)_4$		[4]
Anhydrous Copper Vanadates				
Blossite	Orthorhombic	$Cu_2(V_2O_7)$	Fumarolic	[8]
Ziesite	Monoclinic			[9]
Fingerite	Triclinic	$Cu_{11}(VO_4)_6O_2$		[10]
Mcbirneyite	Triclinic	$Cu_3(VO_4)_2$		[11]
Pseudolyonsite	Monoclinic *			[12]
Borisenkoite	Monoclinic *	$Cu_3[(V,As)O_4]_2$		[13]
Stoiberite	Monoclinic	$Cu_5(VO_4)_2O_2$		[14]

* Borisenkoite has considerable content of As in the V site; the crystal structure of borisenkoite is principally different from mcbirneyite and pseudolyonsite, although both pseydolyonsite and borisenkoite are monoclinic.

Volborthite is interesting not only as a mineral, but also as applied material with functional magnetic, catalytic [15,16] and flame retardant properties. In this mineral Heisenberg kagome antiferromagnet is realized, which may possibly lead to a long sought-after quantum spin-liquid ground state [17,18]. Volborthite is suggested as a novel flame retardant material for polymeric nanocomposites, since its particles form a magnetic barrier layer, and water releases due to mineral dehydration [19]. Moreover, copper vanadates are considered as promising industrial electrodes for application in lithium ion batteries [20]. Blossite, ziesite, mcbirneyite and fingerite show high photoelectroactivity that can be applied for energy storage and conversion [21–23].

The aim of the current study is to understand genetic relations between copper vanadates at room and evaluated temperature. For that we used ex situ and in situ dehydration experiments on volborthite, which led to the formation of the analogues of all natural anhydrous copper vanadates (except for borisenkoite, which is stabilized by the presence of As). The present study can be considered as analyses of phase formation and relation in the Cu-V-O system at different temperatures in situ, and in system, heated to certain temperature and then cooled to the room temperature (ex situ experiments). Both cases may correspond to volcanic environments like fumaroles. The crystal structure complexity can be considered as a numerical reflection of the evolution of atomic arrangement in the Cu-V-O system depending on thermal conditions.

2. Materials and Methods

2.1. Materials

The synthetic reagent with the chemical formula $Cu_3(V_2O_7)(OH)_2 \times 2H_2O$, grade "pure" was obtained from the Ural plant of chemical reagents ("Reachim") and used as the starting material. The preliminary study showed that the reagent is chemically and structurally identical to volborthite, the initial unheated sample is labelled S1 (Sample 1). For clarification of the transformation steps and their reversibility, the material has been studied at elevated temperature using in situ and ex situ strategies. The in situ studies showed that the different phases exist in seven temperature intervals (from room temperature to 800 °C). For each temperature interval, volborthite was annealed at a medium temperature in air atmosphere and used for the ex situ studies. The following samples were used in the study [temperature interval (temperature of ex situ annealing, phase notation)]: 30–230 °C (150 °C, S1), 230–290 °C (250 °C, S2), 290–430 °C (350 °C, S3), 430–510 °C (480 °C, S4), 510–750 °C (650 °C, S5), 750–790 °C (780 °C, S6), >790 °C (850 °C, S7). The samples were annealed in an oven using the following procedure: heating from room temperature to *T* (°C) over 1 h and constant heat treatment at this *T* for 2 h, followed by fast ~20 min or slow above 4 h (up to 10 h depending on annealing temperature) cooling.

2.2. Methods

2.2.1. Chemical Composition

The powder sample used for the study was analyzed with a scanning electron microscope Tescan Vega 3 operating in EDS mode at 20 kV, 1.5 nA and a 5 μm spot-size. The standards used were Cu for Cu, V for V and sanidine for O.

2.2.2. Thermal Analysis

Differential scanning calorimetry (DSC) and thermogravimetric analysis (TG) were carried out using a DSC/TG Netzsch STA 449 F3 instrument (NETZSCH, Selb, Germany) in the 30–1000 °C temperature range at a ramp rate of 10 °C·min^{-1}, gas flow 20 mL/min by heating the samples under Ar atmospheres.

2.2.3. In Situ High-Temperature Powder X-ray Diffraction

In situ high-temperature powder X-ray diffraction (HT XRD) experiments on volborthite were done in air using a Rigaku Ultima IV powder X-ray diffractometer (Co$K\alpha$ radiation, 40 kV/30 mA, Bragg-Brentano geometry, PSD D-Tex Ultra) (Rigaku, Tokyo, Japan) with Rigaku SHT 1500 high-temperature attachment. A thin powder sample was deposited on a Pt sample holder ($20 \times 12 \times 2$ mm^3) from a hexane suspension. Two experiments using different heating strategies were undertaken. In the first one (experiment denoted as HT XRD (I)), the temperature step and the heating rate were 20 °C and 2 °/min, respectively, the experiment was carried out from room temperature up to 800 °C, and the collecting time at each temperature step was about 15 min (scanning velocity 5 °/min). In the second strategy (experiment denoted as HT XRD (II)), the sample was heated to a certain temperature (150, 250, 350, 480, 650, 780 and 850 °C), and the first powder X-ray diffraction pattern was recorded at this temperature one minute after reaching the temperature; then the second pattern was recorded after the sample was kept for 2 h at this temperature. The HT XRD (II) experiment was undertaken in order to obtain more information on kinetic of phase transformation at elevated temperature.

The unit-cell parameters of volborthite and mcbirneyite were refined using the Pawley method implemented in the TOPAS software [24] with the monoclinic structure model of volborthite, space group $C2/m$, with the starting unit-cell parameters a = 10.607, b = 5.864, c = 7.214 Å, β = 94.88°, V = 447.080 Å^3 [25], and triclinic structure model of mcbirneyite, space group P-1, with the starting unit-cell parameters a = 5.196, b = 5.335, c = 6.505 Å, α = 69.22, β = 88.69, γ = 68.08°, V = 155.733 Å^3 [26]. The refinement was based on the reflections in the 2-theta region from 10 to 80°. The backgrounds of volborthite and mcbirneyite

diffraction patterns were modeled using a Chebyshev polynomial approximation of 6th and 8th order, accordingly.

Thermal expansion coefficients were calculated by the DTC and TTT programs [27,28]. The TTT program was also used to determine the orientation of principal axes of the thermal-expansion tensor with respect to the crystallographic axes.

2.2.4. Ex Situ Powder X-ray Diffraction

The phase analysis of all samples obtained in this work (S1–7) by fast cooling was carried out by means of the powder X-ray diffractometer Shimadzu XRD-7000 (SHIMADZU, Kyoto, Japan), using the following conditions: Cu$K\alpha$ radiation, 30 kV/30 mA, scan speed 1°/min, step width 0.1°, 2-theta range 5–65°, room temperature. The powder X-ray diffraction of the samples S1–7 annealed with slow cooling were obtained using the desktop powder diffractometer Rigaku MiniFlex II with Cu$K\alpha$ radiation, 30 kV and 10 mA, scan speed 3°/min, step width 0.02°, 2-theta range 5–65° at room temperature.

2.2.5. Calculations of Crystal-Structure Complexity

In order to investigate the structural complexity of copper vanadates discussed in the present work, we used the approach of numerical evaluation of structural complexity developed by Krivovichev [29–33]. According to this approach, the complexity of crystal structures can be quantitatively characterized by the amount of Shannon information measured in bits (binary digits) per atom (I_G, bits/atom) and per unit cell ($I_{G,total}$, bits/cell), respectively, according to the following Equations:

$$I_G = -\sum_{i=1}^{k} p_i \log_2 p_i \text{ (bits/atom)} \quad (1)$$

$$I_{G,total} = -v\, I_G = -v \sum_{i=1}^{k} p_i \log_2 p_i \text{ (bits/cell)} \quad (2)$$

where k is the number of different crystallographic orbits (independent crystallographic Wyckoff sites) in the structure, and p_i is the random choice probability for an atom from the i-th crystallographic orbit, that is:

$$p_i = m_i/v \quad (3)$$

where m_i is a multiplicity of a crystallographic orbit (i.e., the number of atoms of a specific Wyckoff site in the reduced unit cell), and v is the total number of atoms in the reduced unit cell. It worth noting that the I_G value provides a negative contribution to the configurational entropy (S^{cfg}) of crystalline solids, in accordance with the general principle that the increase in structural complexity corresponds to the decrease in configurational entropy [33]. Structural complexity of copper vanadates was calculated using previously published crystal structure models (*cif*-files), listed in Table 2, and program package ToposPro [34].

Table 2. Crystallographic data and structural complexity for copper vanadates.

Phase	Volborthite	Ziesite	Blossite	Pseudolyonsite	Mcbirneyite	Fingerite	Stoiberite
Chemical formula	$Cu_3(V_2O_7)(OH)_2 \cdot 2H_2O$	$Cu_2(V_2O_7)$		$Cu_3V_2O_8$		$Cu_{11}O_2(VO_4)_6$	$Cu_5O_2(VO_4)_2$
Symmetry	Monoclinic	Monoclinic	Orthorhombic	Monoclinic	Triclinic	Triclinic	Monoclinic
Space group	$C2/m$	$C2/c$	$Fdd2$	$P2_1/c$	$P\text{-}1$	$P\text{-}1$	$P2_1/c$
a (Å)	10.607	7.689	20.676	6.249	5.196	8.158	8.393
b (Å)	5.864	8.029	8.392	7.994	5.355	8.269	6.065
c (Å)	7.214	10.106	6.446	6.378	6.505	8.044	6.446
α (°)	90	90	90	90	69.22	107.1	90
β (°)	94.88	110.252	90	111.49	88.69	91.4	108.09
γ (°)	90	90	90	90	68.08	106.4	90
V (Å^3)	447.08	585.35	1118.46	296.44	155.73	494.12	781.77
Z	2	4	8	2	1	1	4
D_{calc} (g/cm^3)	3.525	3.87	4.051	4.711	4.484	4.774	4.96
I_G (bits/atom)	3.187	2.550	2.550	2.777	2.777	4.450	4.087
$I_{G,total}$ (bits/cell)	70.107	56.107	56.107	72.211	36.106	191.329	277.947
Reference	[25]	[35]	[8]	[36]	[26]	[10]	[37]

3. Results

3.1. Chemical Composition

The study indicated homogeneity of the powder sample S1 with the presence of the following elements in its chemical composition: Cu, V and O with stoichiometry corresponding to volborthite.

3.2. In Situ High-Temperature Powder X-ray Diffraction

The HT XRD (I) (Figure 1) showed that synthetic analogue of volborthite is stable from room temperature to 230 °C, when it transforms into an X-ray amorphous phase. Starting from 290 °C, the reflections of ziesite and tenorite are found, which are stable up to 510 °C. The reflections of pseudolyonsite are observed from 430 to 510 °C, their intensities decrease upon increasing the temperature. Mcbirneyite reflections appear at 430 °C and the phase is stable up to 750 °C. The phase or phases existing in the range 750–790 °C could not be identified using known data. Only a few reflections are registered at 790–800 °C, which have been indexed as copper and vanadium oxides (Table 3).

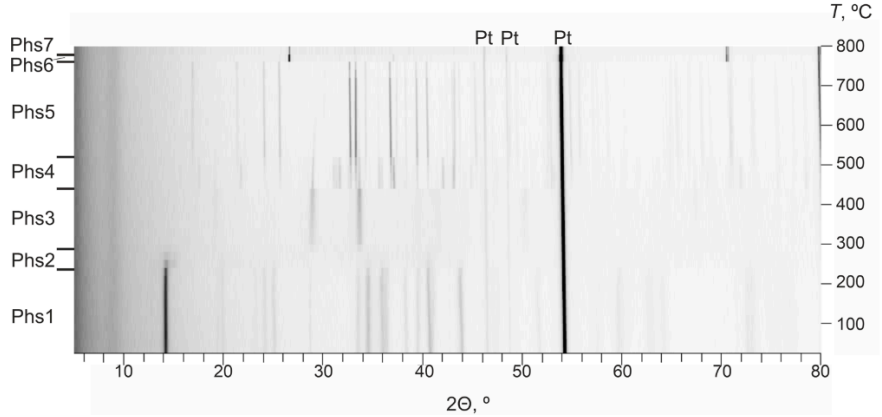

Figure 1. HT XRD (I) from 30 to 800 °C: 30–230 °C—volborthite, 230–290 °C—X-ray amorphous phase, 290–430 °C—ziesite and tenorite, 430–510 °C—ziesite, tenorite, pseudolyonsite and mcbirneyite, 510–750 °C—mcbirneyite, 750–790 °C—unidentified phase, 790–800 °C—copper and vanadium oxides.

Table 3. Phase evolution from volborthite.

Temperature Range (Temperature of Annealing), °C	In Situ Phase (HT XRD (I))	In Situ Phase (HT XRD (II))	Phase Notation	Ex Situ Phase (Annealing in Oven with Fast Cooling)	Ex Situ Phase (Annealing in Oven with Slow Cooling)
30–230 (150)	Volborthite	Volborthite	S1	Volborthite	Volborthite
230–290 (250)	Volborthite, X-ray amorphous phase	Volborthite, X-ray amorphous phase	S2	Volborthite, fingerite, karelianite	Volborthite, fingerite
290–430 (350)	Ziesite and tenorite	Ziesite and tenorite	S3	Ziesite and tenorite	Ziesite and tenorite
430–510 (480)	Ziesite, tenorite, pseudolyonsite and mcbirneyite	Mcbirneyite, ziesite, pseudolyonsite, blossite and fingerite	S4	Mcbirneyite, ziesite, pseudolyonsite and fingerite	Mcbirneyite, ziesite, pseudolyonsite, blossite and fingerite
510–750 (650)	Mcbirneyite	Mcbirneyite, blossite	S5	Mcbirneyite and ziesite	Mcbirneyite, blossite and ziesite
750–790 (780)	Unidentified phase	Unidentified phase	S6	Mcbirneyite, shcherbinaite, ziesite and tenorite	Mcbirneyite, stoiberite, ziesite and blossite
790–800 (850)	Copper and vanadium oxides	X-ray amorphous phase	S7	α-$CuVO_3$, ziesite, fingerite, Cu_3VO_4	Mcbirneyite, stoiberite, ziesite, α-$CuVO_3$, VO_2

The HT XRD (II) showed that both patterns recorded just after reaching 150 °C and after 2 h at this temperature correspond to volborthite (Figure 2). The pattern recorded at 250 °C corresponds to low-crystallinity volborthite that is characterized by the absence of some reflections and reflections broadening (Figure 2). The observed split of the first and the most intensive reflection marks the contraction of volborthite basal spacing, possibly as the result of its dehydration and dehydroxylation, which precedes the decomposition of the mineral. The main difference between patterns recorded just after reaching 250 °C and after 2 h of heating is that volborthite crystallinity decreased. Patterns recorded at 350 °C immediately and after 2 h are identical, and correspond to ziesite with traces of tenorite. Patterns recorded at 480 °C immediately and after 2 h are also identical, and correspond to a mixture of mcbirneyite, fingerite, ziesite, pseudolyonsite and blossite. The main phase at patterns recorded just after reaching 650 °C and after 2 h heating is mcbirneyite. The distinction between these patterns is the presence of the low-intensity reflection at ~33 °C in 2-theta that has been identified as blossite (Figure 2). The patterns recorded at 780 °C contain the only reflection that has not been identified. The patterns recorded at 850 °C do not contain any reflections (Figure 2).

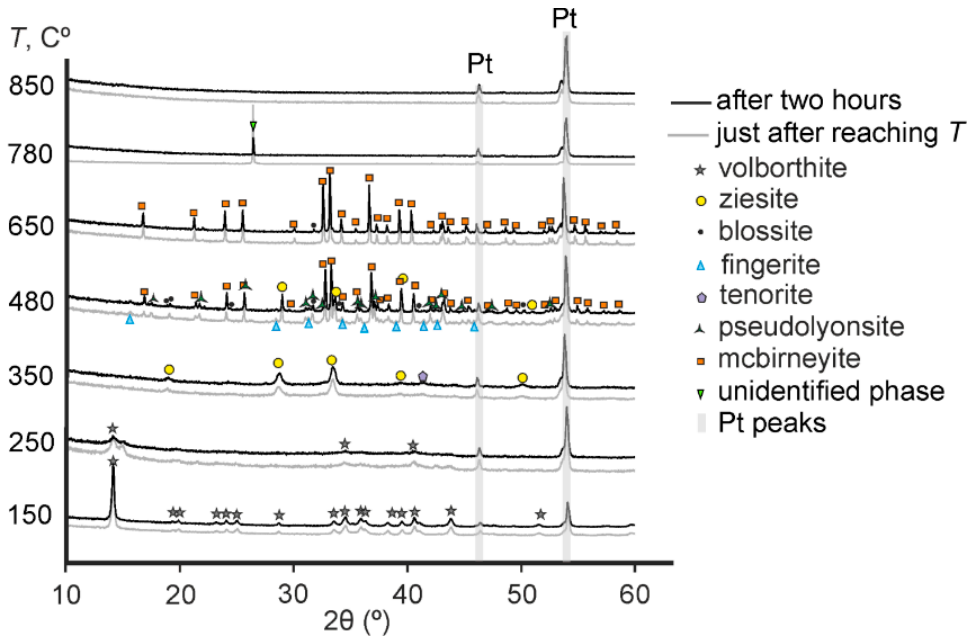

Figure 2. HT XRD (II) steps: 150 °C—volborthite; 250 °C—low-crystallinity volborthite; 350 °C—ziesite with traces of tenorite; 480 °C—mcbirneyite, fingerite, pseudolyonsite, ziesite and blossite; 650 °C—mcbirneyite (just after reaching temperature) and mcbirneyite with traces of blossite (after 2 h); 780 °C—one reflection of unidentified phase; 850 °C—absence of reflections. Pt—sample holder.

3.3. Thermal Analysis

Synthetic analogue of volborthite demonstrates two major mass losses and five thermal events in the temperature range from 25 to 1000 °C (Figure 3). The first mass loss is by 11.55%, appears in the interval from 30 to ~340 °C and is accompanied by the endothermal effect at 210.2 °C. This mass loss corresponds to the complete dehydration (the loss of H_2O molecules) and dehydroxylation (the loss of OH-groups) corresponding to the peak at 210.2 °C. Ziesite and tenorite crystallize at ~300 °C producing the exothermal effect at 304.3 °C. The strong exothermal effect at 452.9 °C, and the following weak endothermal effect at 481.3 °C, appear without mass changes and are assigned as the formation of pseudolyonsite and mcbirneyite, respectively. The second mass loss is of 4.87%, and appears from 700 to 800 °C, accompanied by an exothermal effect at 746.8 °C, which most

likely corresponds to the decomposition of copper vanadate and the loss of some oxygen. Generally, the results are in agreement with previous studies [2,38].

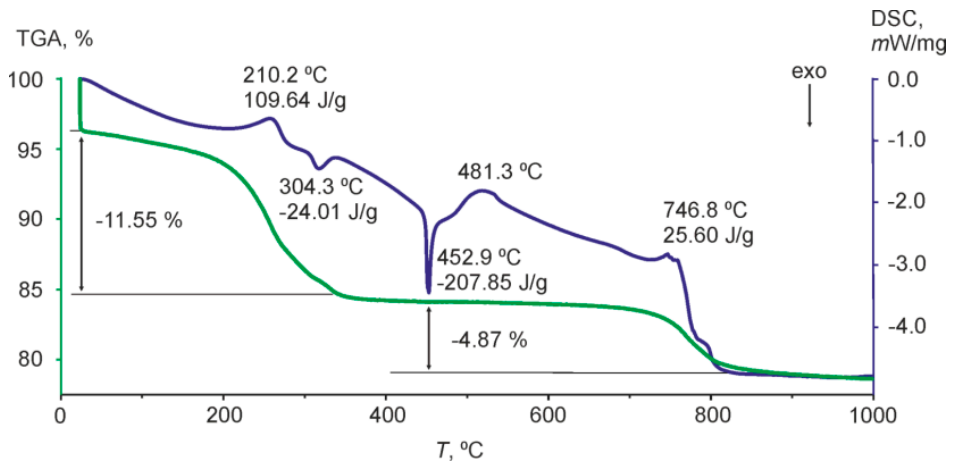

Figure 3. Thermal analyses: differential scanning calorimetry curve-blue, thermal gravimetric analyses curve-green.

3.4. Phases Obtained by Ex Situ Annealing

The diffraction pattern of S1 corresponds to that of volborthite. The S2 diffraction pattern contains the reflections of volborthite, fingerite and karelianite in the case of fast cooling, and the reflections of volborthite and fingerite in the case of slow cooling. The S3 mixture consists of ziesite and tenorite in both cases, which is in agreement with the in situ studies of volborthite (Table 3). Pseudolyonsite, mcbirneyite and fingerite appear in S4 in addition to ziesite. A small amount of blossite crystallized only during slow cooling. Mcbirneyite and a small amount of ziesite are identified in the sample S5 of both fast and slow cooling; stoiberite and blossite are identified in S5 cooled slowly. Shcherbinaite, V_2O_5, is registered in association with mcbirneyite, ziesite and tenorite in the sample S6, forming after heating up to 780 °C and fast cooling. Stoiberite and blossite were formed during slow cooling in the sample S6 in association with mcbirneyite and ziesite. Fingerite, ziesite, α-$CuVO_3$ and Cu_3VO_4 are identified in the sample S7 with fast cooling, whereas mcbirneyite, stoiberite, ziesite, α-$CuVO_3$ and VO_2 are identified in the sample S7 with slow cooling (Table 3, Figure 4).

3.5. Thermal Expansion Coefficients of Volborthite and Mcbirneyite at Elevated Temperatures

The refinement of the unit-cell parameters was done in the temperature ranges 25–220 °C for volborthite and 520–740 °C for mcbirneyite (Figure 5). Thermal expansion coefficients of volborthite (at 100 °C) and mcbirneyite (at 650 °C) are given in Table 4 and compared to that reported previously [2]. Thermal expansion of volborthite is strongly anysotropic in the plane of monoclinicity ac, that could be interpreted as a typical monoclinic shear deformation [39]. The contraction of the c unit cell parameter reflects sample dehydration and dehydroxylation (Figure 5). Thermal expansion of mcbirneyite is also anisotropic, with the $\alpha_{max}/\alpha_{min}$ value equal to 15.6 (Table 4). The thermal expansion coefficients along a and b crystallographic axes, i.e., α_a and α_b, are nearly identical ~11×10^6 °C^{-1} and correspond to the plane of CuO_4 sqares. The α_c coefficient oriented perpendicularly to CuO_4 layers is much smaller, 0.7×10^6 °C^{-1}. Based on that, the anisopropy of thermal expansion is interpreted as anisotropy in the three-dimensional distribution of Cu-O bonds.

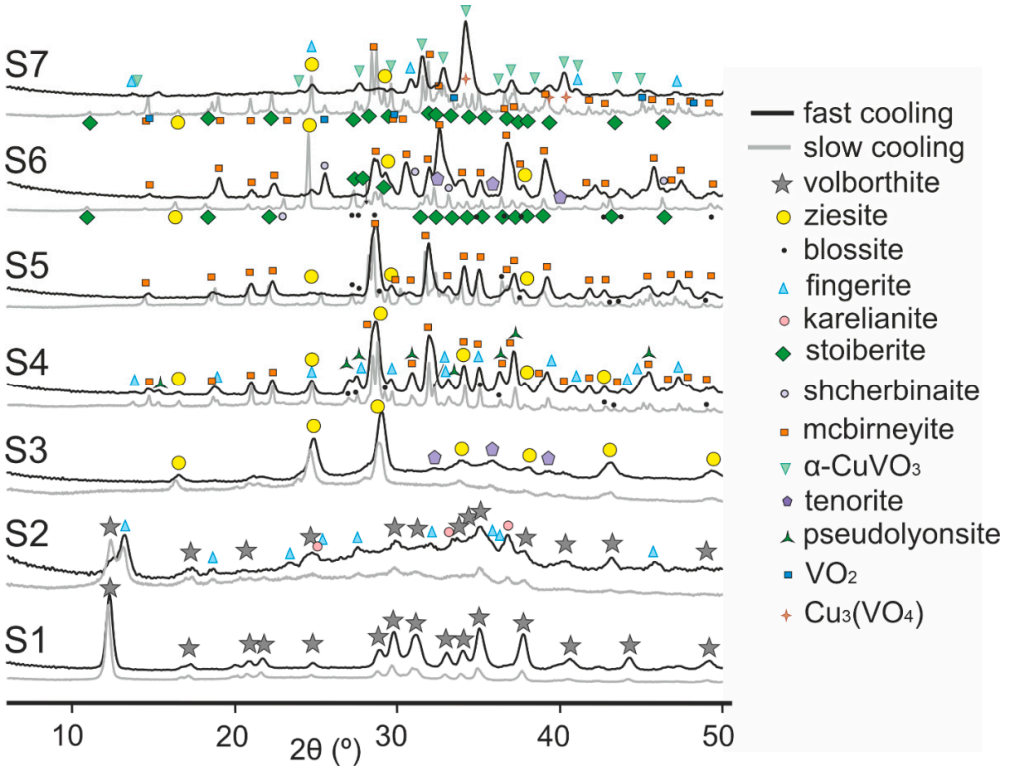

Figure 4. X-ray diffraction patterns of samples heated ex situ and cooled fast and slow to the room temperature. Note, karelianite, $V^{3+}{}_2O_3$; shcherbinaite, $V^{5+}{}_2O_5$; tenorite, CuO. The temperatures of annealing are 150 °C (S1), 250 °C (S2), 350 °C (S3), 480 °C (S4), 650 °C (S5), 780 °C (S6), 850 °C (S7).

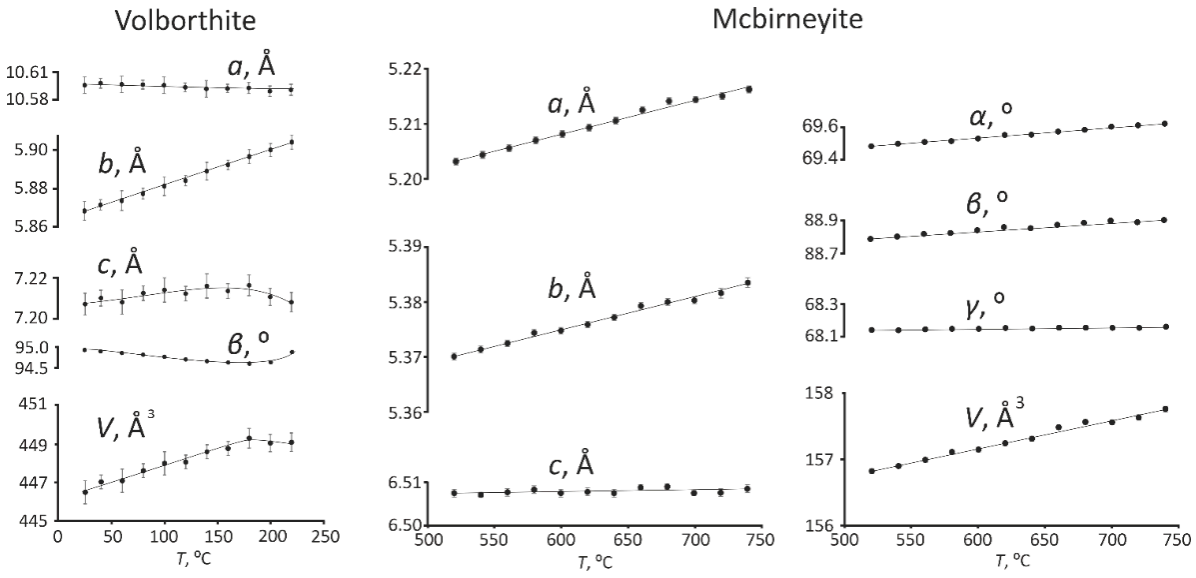

Figure 5. Unit cell parameters of volborthite in the temperature range 25–220 °C and mcbirneyite in the temperature range 520–740 °C.

Table 4. The main characteristics of thermal expansion/contraction of volborthite (at 100 °C) and mcbirneyite (at 650 °C), $\times 10^6$ °C^{-1}.

Phase	α_1	α_2	α_3	$<\alpha_{1a}$	$<\alpha_{2b}$	$<\alpha_{3c}$	α_a	α_b	α_c	α_α	α_β	α_γ	α_V
Volborthite	−16.5(1.3)	30.7(2.5)	20.7(1.7)	35.3	0	39.9	−4.1(6)	30.7(7)	5.4(1.5)	-	−21.6(4)	-	34.9(2.5)
Volborthite *	−21.9(1)	28.8(1)	22.6(1)	39.1	0	43.9	−4.2(5)	28.7(5)	1.2(8)	-	−26.7(1)	-	29.5(1)
Mcbirneyite	12.4(4)	15.8(6)	−1.01(4)	36.7	35.7	19.7	11.6(3)	11.0(4)	0.7(4)	8.8(2)	6.0(3)	1.2(1)	27.2(1.0)

α—coefficient of thermal expansion [α_1, α_2, α_3—eigenvalues (main values); α_a, α_b, α_c—values along crystallographic axes], $<\alpha_{1a}$—angle between axes α_1 and *a*. * Thermal expansion characteristics of volborthite from the Tyuya-Muyun Deposit, Kyrgyzstan [2].

3.6. Crystal Structure Complexity

Crystal structure complexity of volborthite, ziesite, blossite, mcbirneyite, pseudolyonsite, fingerite and stoiberite are shown at Table 2, as well as crystal structure data used for calculation.

4. Discussion

4.1. General Trend of High-Temperature Transformation

Volborthite is stable up to ~230 °C, when it transforms to an X-ray amorphous phase as a result of dehydration and dehydroxylation. Starting from 290 °C, ziesite and tenorite crystallize; at temperatures above 430 °C, two polymorphs of $Cu_3(VO_4)_2$: pseudolyonsite (denoted as α-modification) and mcbirneyite (denoted as β-modification) coexist with ziesite and tenorite up to ~510 °C. In the temperature range 510–750 °C, only mcbirneyite is observed. The schematic transformation steps according to the in situ study are as follows: $Cu_3(V_2O_7)(OH)_2{\cdot}2H_2O$ (volborthite) → X-ray amorphous phase → β-$Cu_2(V_2O_7)$ (ziesite) + CuO (tenorite) → β-$Cu_2(V_2O_7)$ (ziesite) + CuO (tenorite) + α-$Cu_3(VO_4)_2$ (pseudolyonsite) + β-$Cu_3(VO_4)_2$ (mcbirneyite) → β-$Cu_3(VO_4)_2$ (mcbirneyite). The thermal analysis data agree with the aforementioned phase transformation (Figure 6). The presence of tenorite is due to the difference in Cu:V ratio between copper vanadates.

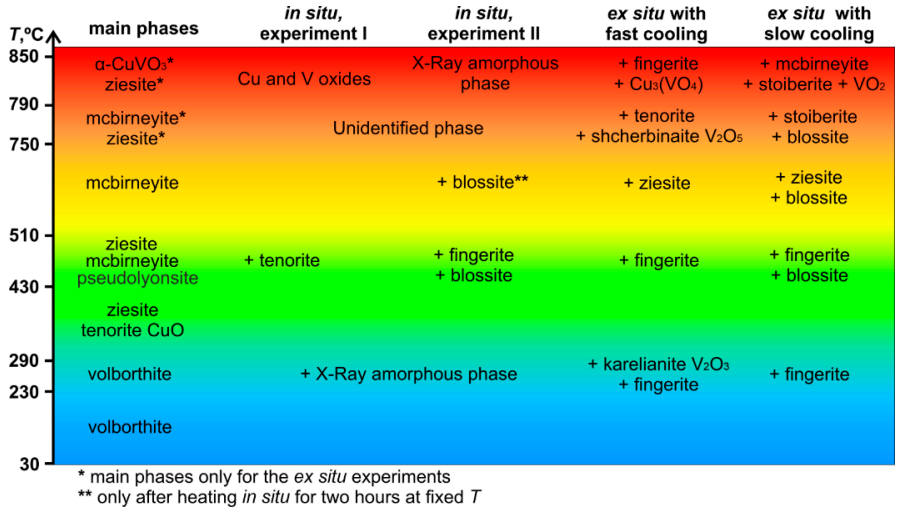

Figure 6. Scheme of volborthite transformation as the function of temperature.

The results of the ex situ experiments show that the main sets of phases agree with those observed by in situ techniques: volborthite, ziesite, mcbirneyite and pseudolyonsite have been identified in different temperature ranges (Table 3). However, the number of phases observed for each temperature range is higher in the case of the ex situ annealing compared to the in situ study. For example, only mcbirneyite has been identified by the in situ high-temperature powder X-ray diffraction in the temperature range 510–750 °C, whereas, in the sample S5 (annealed at 650 °C), this phase occurs together with ziesite (for fast cooling) or with ziesite and blossite (for slow cooling) (Table 3). A wider variety of ex situ phases is explained by the passage of the system through energy minimums with

decreasing temperature, which leads to the crystallization of a number of compounds that are unstable at high temperatures. The schematic transformation steps according to the ex situ annealing with fast cooling are as following: volborthite → volborthite + fingerite → ziesite + tenorite → ziesite + fingerite + pseudolyonsite + mcbirneyite → mcbirneyite + ziesite → mcbirneyite + V_2O_5 + ziesite + tenorite → α-$CuVO_3$ + ziesite + fingerite + Cu_3VO_4 (Figure 6).

Phase composition of the compounds formed during the ex situ annealing followed by slow cooling is more complex: volborthite → volborthite + fingerite → ziesite + tenorite → blossite + ziesite + fingerite + pseudolyonsite + mcbirneyite → mcbirneyite + ziesite + blossite → mcbirneyite + ziesite + blossite + stoiberite → mcbirneyite + ziesite + stoiberite + α-$CuVO_3$ + VO_2 (Figure 6).

It is interesting to note that, among the identified phases (Figure 4, Table 3), three compounds: VO_2, α-$CuVO_3$, Cu_3VO_4 have not been found in nature. Our experiments show that these phases can possibly form at fumaroles of Tolbachik and Izalco volcanoes, where the association of natural copper vandates is found, however the temperature of formation of these phases is high (~about 850 °C), which is obviously an obstacle to the detection and characterization of such phases.

4.2. The Influence of Heating Strategy to the Phase Composition

The results on dehydration and dehydroxylation of volborthite are unexpected, since all known anhydrous copper vanadates found in nature (with exception to borisenkite that require some As) were obtained in heating experiments. The experimental observation is consistent with natural processes, since anhydrous copper vanadates are known in only two fumaroles, but form a relatively rich mineral diversity: five species are found on Izalco volcano and six minerals are described at Tolbachik volcano (Table 1). The aforementioned results suggest that all copper vanadates involved in the study (see Table 3) are stable at room temperature, because they have been identified in the samples annealed ex situ and cooled to room temperature.

The ex situ experiments show more complex phase composition in comparison to the in situ experiments. It is noteworthy that samples annealed ex situ also significantly differ by their phase composition depending on the cooling rate: richer phase composition is characteristic for slow cooling. For example, stoiberite has been identified only in samples annealed ex situ that were slowly cooled to room temperature. The comparison of the phase composition for annealed samples (Figure 4) cooled fast and slow shows that the main difference is observed above 430 °C, i.e., for the samples S4, S5, S6 and S7. This can be explained by the existence of several possible energy minima for the Cu-V-O system cooling down from temperature above 430 °C to room temperature. Based on that, we can suggest that in the case of copper vanadates the phase composition is determined not only by temperature, but by kinetic of heating and cooling. To check this suggestion, we performed the HT XRD (II) experiment where the pattern has been recorded immediately after reaching a certain temperature and after 2 h of heating. The comparison of patterns obtained at the same temperature but with different heating time shows an absence of phase evolution during the time (Figure 2). The only difference is the appearance of low-intensity reflection (~33 ° in 2-theta) in the sample kept at 650 °C, in comparison to the pattern recorded immediately after reaching 650 °C.

However, if we compare results from the HT XRD (I) and (II) experiments (Figure 6), we can see that the difference in the phase composition is observed above 430 °C, similarly to the ex situ experiments (Figures 4 and 6). Therefore, in the HT XRD (I) ziesite, mcbirneyite and pseudolyonsite were obtained in the temperature range 430–510 °C, while in the HT XRD (II) fingerite and blossite are found in addition to these phases at 480 °C. At temperatures above 510 °C, only mcbirneyite is found in HT XRD (I), whereas in HT XRD (II), low-intensity reflection of blossite appeared in addition to mcbirneyite after 2 h of heating. Moreover, the comparison of our results [HT XRD (I) and (II)] to recently published materials on volborthite from Tyuya-Muyun Deposit, Kyrgyzstan [2] also shows

the main difference in phase composition, since they reported the appearance of fingerite and stoiberite above 760 °C, while we have observed these phases only in the samples annealed ex situ (Table 3, Figure 6). Moreover, in that study [2], blossite was not detected in the in situ heating of volborthite. The evolution of the phase composition of the samples held for short and prolonged times (in HT XRD (II)) at the same temperature in situ has not been detected (with the exception of the appearance of one low-intensity reflection). The difference in phase composition between the HT XRD (I) and (II) experiments is more significant.

The general steps of the phase evolution from volborthite according to our and previous study [2] are volborthite → X-ray amorphous phase → ziesite → ziesite + mcbirneyite + pseudolyonsite → mcbirneyite. In this case, the conditions leading to the formation of blossite, fingerite and stoiberite are not entirely clear, since in different experiments these phases were encountered in different temperature ranges (or not at all). The phase formation can be controlled by the kinetic factors (like heating and cooling rate), i.e., subtle changes in the thermal regime.

4.3. Crystal Structure Complexity of Copper Vanadates

It is interesting to consider the crystal structure complexity for the vanadate phases obtained in this study. Mcbirneyite is a high-temperature polymorph of pseudolyonsite (Table 2). In agreement with the general tendency that high-temperature phases are structurally simpler than their low-temperature counterparts [30], pseudolyonsite is more complex and has higher symmetry (monoclinic, D_{calc} = 4.711 g/cm^3, $I_{G,total}$ = 72.211 bits/cell) in comparison to mcbirneyite (triclinic, D_{calc} = 4.484 g/cm^3, $I_{G,total}$ = 36.106 bits/cell). The two $Cu_2V_2O_7$ polymorphs, ziesite and blossite, have the same crystal structure complexity ($I_{G,total}$ = 56.107 bits/cell), although ziesite has lower symmetry (monoclinic, D_{calc} = 3.87 g/cm^3) than blossite (orthorhombic, D_{calc} = 4.051 g/cm^3). Blossite formation conditions are the most incomprehensible: it appeared above 430 °C in HT XRD (II), then disappeared and appeared again at the prolonged heating of mcbirneyite; blossite is also found in ex situ experiments with slow cooling. It is remarkable that both pairs of polymorphs, i.e., mcbirneyite and pseudolyonsite, and ziesite and blossite, violate the principle of symmetry increasing with temperature, as outlined by Filatov [39]. In contrast, structural complexity parameters appear to be more sensitive to the temperature changes, indicating that symmetry is only one part of the structural complexity, which also depends upon the size of the system, i.e., the number of atoms in a reduced unit cell [29].

In this work, we have observed a decreasing trend in crystal structure complexity of the main phases forming during in situ heating experiments with increasing temperature: volborthite, $I_{G,total}$ = 70 bits/cell → ziesite, $I_{G,total}$ = 56 bits/cell → mcbirneyite, $I_{G,total}$ = 36 bits/cell, except for pseudolyonsite, $I_{G,total}$ = 72 bits/cell, that exists at temperature range 430–510 °C with other phases. There is also a trend that the longer the sample cools, the more complex the crystal structures that are formed, which agrees with the Goldsmith principle that kinetically stabilized phases are usually simpler than their thermodynamically stable counterparts [30,40]. All samples obtained by the in situ heating have a structural complexity less than 80 bits/cell, while fingerite obtained by the ex situ heating and fast cooling has a structural complexity of 191 bits/cell. Stoiberite obtained by ex situ heating and slow cooling is even more complex with $I_{G,total}$ = 278 bits/cell. An exception to this trend is blossite that forms in the ex situ experiment with slow cooling, although its crystal structure is not so complex, 56 bits/cell (Table 4). Perhaps this exception is due to the fact that blossite and ziesite are polymorphs with identical structural complexities (Table 2). The high complexity of fingerite and stoiberite may explain the 'ephemeral' (different results in different experiments) conditions of their formation; the difference in the Cu:V ratio (Table 1) may also be responsible for this.

5. Conclusions

1. The in situ heating of volborthite showed the following evolution steps: volborthite (S1) → X-ray amorphous phase (S2) → ziesite + tenorite (S3) → ziesite + tenorite + pseudolyonsite + mcbirneyite (S4) → mcbirneyite (S5) or in chemical composition: $Cu_3(V_2O_7)(OH)_2 \cdot 2H_2O$ → X-ray amorphous phase → β-$Cu_2(V_2O_7)$ + CuO → β-$Cu_2(V_2O_7)$ + CuO + α-$Cu_3(VO_4)_2$ + β-$Cu_3(VO_4)_2$ → β-$Cu_3(VO_4)_2$.

2. The comparison of patterns obtained in situ at the same temperatures, but different heating times, showed an absence of phase evolution during the time, except for the appearance of trace blossite after 2 h of heating at 650 °C.

3. The ex situ annealing of volborthite followed by fast cooling showed the same trend of phase evolution as for the in situ experiments. However, the phase composition turned out to be more complex: fingerite and karelianite (S2), fingerite (S4), ziesite (S5) were found in addition to those observed for the corresponding steps of the in situ experiments. Mcbirneyite, shcherbinaite, ziesite and tenorite were identified in S6, whereas α-$CuVO_3$, ziesite, fingerite, Cu_3VO were found in S7, in contrast with the in situ experiments.

4. The ex situ annealing of volborthite, followed by slow cooling, showed an even more complex composition: blossite was registered in S4, S5 and S6, whereas stoiberite was found in S6 and S7 in addition to other phases mentioned above.

5. The in situ thermal analyses shows the mass loss of 11.55% in the interval 30–340 °C, and an endothermal effect at 210.2 °C that corresponds to the complete dehydration and dehydroxylation of volborthite. Ziesite and tenorite crystallize at ~300 °C, producing the exothermal effect at 304.3 °C. The exothermal effect at 452.9 °C, followed by a weak endothermal effect at 481.3 °C, are assigned to the formation of pseudolyonsite and mcbirneyite, respectively. The mass loss of 4.87% appears from 700 to 800 °C, accompanied by an exothermal effect at 746.8 °C which, most likely, corresponds to the decomposition of copper vanadate.

6. The comparison of the phase composition for the annealed samples cooled fast and slow shows that the main difference in the phase composition is observed above 430 °C, i.e., for S4 (480 °C), S5 (650 °C), S6 (780 °C) and S7 (850 °C), and they affect the formation of blossite, fingerite and stoiberite. This can be regarded as being due to the existence of many possible energy minima (phase formation) for the cooling Cu-V-O system.

7. The results of in situ experiments with various strategies also differ in the phase composition above 430 °C, similarly to ex situ experiments, that confirms the idea of many possible energy minima (phase formation) for Cu-V-O system.

8. The phases VO_2, α-$CuVO_3$, Cu_3VO_4 can possibly form under natural conditions (as minerals) in fumaroles at temperatures ~850 °C.

9. We have observed the tendency of decreasing structural complexity of the main phases forming during in situ heating experiments with increasing temperature: volborthite → ziesite → mcbirneyite. There is also a trend that the longer the sample cools, the more complex the crystal structures that are formed, which agrees with the Goldsmith principle that kinetically stabilized phases are usually simpler than their thermodynamically stable counterparts. An exception to the latter trend is blossite, perhaps because blossite and ziesite are polymorphs with identical crystal structure complexity.

10. The high complexity of fingerite and stoiberite may explain the 'ephemeral' (different results in different experiments) conditions of their formation; the difference in the Cu:V ratio may also be responsible for this.

Author Contributions: Conceptualization, E.S.Z. and R.M.I.; methodology, R.M.I., E.S.Z., A.V.S., A.A.N., M.G.K., M.A.N., A.A.Z. and D.S.B.; software, R.M.I., A.A.N., M.G.K., M.A.N., A.N.K. and R.A.K.; validation, R.M.I., E.S.Z., S.V.K., A.V.S., A.A.N., M.A.N. and A.V.K.; formal analysis, R.M.I., A.A.N., L.P.A., M.G.K., M.A.N., A.N.K. and D.A.K.; data curation, E.S.Z., S.V.K., L.P.A. and M.G.K.; writing—original draft preparation, E.S.Z. and R.M.I.; writing—review and editing, R.M.I., E.S.Z., S.V.K., A.V.S., A.A.N., L.P.A., M.G.K., M.A.N., A.N.K., A.A.Z., A.V.K., D.S.B., R.A.K. and D.A.K.; visualization, R.M.I., E.S.Z., A.A.N. and A.N.K.; supervision, E.S.Z.; project administration, E.S.Z.; funding acquisition, E.S.Z. and S.V.K. All authors have read and agreed to the published version of the manuscript.

Funding: This research was funded by Russian Fund for Basic Research, grant number 20-35-70008 for evolution of mineral composition with temperature and Russian Science Fund, grant number 19-17-00038 for crystal structure complexity.

Acknowledgments: The studies in this work were carried out using the equipment of the Centre for X-ray Diffraction Studies of Saint Petersburg State University and Analytical Centre of Institute of Volcanology and Seismology FEB RAS. The DSC/TG Netzsch STA 449 F3 instrument was obtained by the Nauka program.

Conflicts of Interest: The authors declare no conflict of interest.

References

1. Volborth, A.; Hess, H. Ueber (das Volborthit), ein neues Vanadhaltiges Mineral. *Bull. Académie Impériale Sci. St.-Pétersbourg* **1838**, *4*, 21–23.
2. Ginga, V.A.; Siidra, O.I.; Ugolkov, V.L.; Bubnova, R.S. Refinement of the Crystal Structure and Features of the Thermal Behavior of Volborthite $Cu_3V_2O_7(OH)_2{\cdot}2H_2O$ from the Tyuya-Muyun Deposit, Kyrgyzstan. *Zapiski Rossiyskogo Mineralogicheskogo Obshchestva* **2021**, *150*, 115–133. (In Russian) [CrossRef]
3. Hålenius, U.; Hatert, F.; Pasero, M.; Mills, S.J. New minerals and nomenclature modifications approved in 2016. *Mineral. Mag.* **2016**, *80*, 1135–1144. [CrossRef]
4. Nenadkevich, K.A. Turanite and alaite, two new vanadium minerals. *Bull. Académie Impériale Sci. St.-Pétersbourg* **1909**, *3*, 185–187.
5. Zhitova, E.S.; Anikin, L.P.; Sergeeva, A.V.; Ismagilova, R.M.; Rashidov, V.A.; Chubarov, V.M.; Kupchinenko, A.N. Volborthite Occurrence at the Alaid Volcano (Atlasov Island, Kuril Islands, Russia). *Zapiski Rossiyskogo Mineralogicheskogo Obshchestva* **2020**, *149*, 78–95. (In Russian) [CrossRef]
6. Balassone, G.; Petti, C.; Mondillo, N.; Panikorovskii, T.L.; de Gennaro, R.; Cappelletti, P.; Altomare, A.; Corriero, N.; Cangiano, M.; D'Orazio, L. Copper minerals at Vesuvius Volcano (Southern Italy): A mineralogical review. *Minerals* **2019**, *9*, 730. [CrossRef]
7. Pekov, I.V.; Zubkova, N.V.; Yapaskurt, V.O.; Polekhovsky, Y.S.; Britvin, S.N.; Turchkova, A.G.; Sidorov, E.G.; Pushcharovsky, D.Y. Kainotropite, $Cu_4Fe^{3+}O_2(V_2O_7)(VO_4)$, a new mineral with a complex vanadate anion from fumarolic exhalations of the Tolbachik Volcano, Kamchatka, Russia. *Canad. Miner.* **2020**, *58*, 155–165. [CrossRef]
8. Robinson, P.D.; Hughes, J.M.; Malinconico, M.L. Blossite, α-$Cu^{2+}{}_2V^{5+}{}_2O_7$, a new fumarolic sublimate from Izalco volcano, El Salvador. *Am. Mineral.* **1987**, *72*, 397–400.
9. Hughes, J.M.; Birnie, R.W. Ziesite, ß-$Cu_2V_2O_7$, a new copper vanadate and fumarole temperature indicator. *Am. Mineral.* **1980**, *65*, 1146–1149.
10. Finger, L.W. Fingerite, $Cu_{11}O_2(VO_4)_6$, a new vanadium sublimate from Izalco volcano, El Salvador: Crystal structure. *Am. Mineral.* **1985**, *70*, 197–199.
11. Hughes, J.M.; Christian, B.S.; Finger, L.W.; Malinconico, L.L. Mcbirneyite, $Cu_3(VO_4)_2$, a new sublimate mineral from the fumaroles of Izalco volcano, El Salvador. *J. Volcanol. Geotherm. Res.* **1987**, *33*, 183–190. [CrossRef]
12. Zelenski, M.E.; Zubkova, N.V.; Pekov, I.V.; Boldyreva, M.M.; Pushcharovsky, D.Y.; Nekrasov, A.N. Pseudolyonsite, $Cu_3(VO_4)_2$, a new mineral species from the Tolbachik volcano, Kamchatka Peninsula, Russia. *Eur. J. Mineral.* **2011**, *23*, 475–481. [CrossRef]
13. Pekov, I.V.; Zubkova, N.V.; Yapaskurt, V.O.; Polekhovsky, Y.S.; Vigasina, M.F.; Britvin, S.N.; Turchkova, A.G.; Sidorov, E.G.; Pushcharovsky, D.Y. A new mineral borisenkoite, $Cu_3[(V,As)O_4]_2$, and the isomorphous series borisenkoite–lammerite-β in fumarolic exhalations of the Tolbachik volcano, Kamchatka, Russia. *Phys. Chem. Miner.* **2020**, *47*, 17. [CrossRef]
14. Birnie, R.W.; Hughes, J.M. Stoiberite, $Cu_5V_2O_{10}$, a new copper vanadate from Izalco volcano, El Salvador, Central America. *Am. Mineral.* **1979**, *64*, 941–944.
15. Palacio, L.A.; Silva, J.M.; Ribeiro, F.R.; Ribeiro, M.F. Catalytic oxidation of volatile organic compounds with a new precursor type copper vanadate. *Catal. Today* **2008**, *133*, 502–508. [CrossRef]
16. Zhao, X.; Huang, L.; Li, H.; Hu, H.; Han, J.; Shi, L.; Zhang, D. Highly dispersed V_2O_5/TiO_2 modified with transition metals (Cu, Fe, Mn, Co) as efficient catalysts for the selective reduction of NO with NH_3. *Chin. J. Catal.* **2015**, *36*, 1886–1899. [CrossRef]
17. Yoshida, H.; Okamoto, Y.; Tayama, T.; Sakakibara, T.; Tokunaga, M.; Matsuo, A.; Narumi, Y.; Kindo, K.; Yoshida, M.; Takigawa, M.; et al. Magnetization "steps" on a kagome lattice in volborthite. *J. Phys. Soc. Jpn.* **2009**, *78*, 043704. [CrossRef]

18. Hiroi, Z.; Ishikawa, H.; Yoshida, H.; Yamaura, J.I.; Okamoto, Y. Orbital transitions and frustrated magnetism in the kagome-type copper mineral volborthite. *Inorg. Chem.* **2019**, *58*, 11949–11960. [CrossRef]
19. Ghiyasiyan-Arani, M.; Masjedi-Arani, M.; Ghanbari, D.; Bagheri, S.; Salavati-Niasari, M. Novel chemical synthesis and characterization of copper pyrovanadate nanoparticles and its influence on the flame retardancy of polymeric nanocomposites. *Sci. Rep.* **2016**, *6*, 1–9.
20. Fan, Z.; Yang, X.; Li, G.; Zhao, Y.; Shen, J. Preparation and properties of copper vanadate materials. *J. Adv. Phys. Chem.* **2015**, *4*, 52–65. [CrossRef]
21. Newhouse, P.F.; Boyd, D.A.; Shinde, A.; Guevarra, D.; Zhou, L.; Soedarmadji, E.; Li, G.; Neaton, J.B.; Gregoire, J.M. Solar fuel photoanodes prepared by inkjet printing of copper vanadates. *J. Mater. Chem. A* **2016**, *4*, 7483–7494. [CrossRef]
22. Zhou, L.; Yan, Q.; Shinde, A.; Guevarra, D.; Newhouse, P.F.; Becerra-Stasiewicz, N.; Chatman, S.M.; Haber, J.A.; Neaton, J.B.; Gregoire, J.M. High throughput discovery of solar fuels photoanodes in the CuO–V_2O_5 system. *Adv. Energy Mater.* **2015**, *5*, 1500968. [CrossRef]
23. Hossain, M.K.; Sotelo, P.; Sarker, H.P.; Galante, M.T.; Kormányos, A.; Longo, C.; Macaluso, R.T.; Huda, M.N.; Janáky, C.; Rajeshwar, K. Rapid one-pot synthesis and photoelectrochemical properties of copper vanadates. *ACS Appl. Energy Mater.* **2019**, *2*, 2837–2847. [CrossRef]
24. Bruker-AXS. *TopasV4.2: General Profile and Structure Analysis Software for Powder Diffraction Data*; Bruker-AXS: Karlsruhe, Germany, 2009.
25. Lafontaine, M.A.; Le Bail, A.; Férey, G. Copper-containing minerals—I. $Cu_3V_2O_7(OH)_2.2H_2O$: The synthetic homolog of volborthite; Crystal structure determination from X-ray and neutron data; Structural correlations. *J. Solid State Chem.* **1990**, *85*, 220–227. [CrossRef]
26. Coing-Boyat, J. Structure de la variete ordinaire, triclinique, de l'orthovanadate de cuivre(II), $Cu_3(VO_4)_2$. *Acta Cryst.* **1982**, *B38*, 1546–1548. [CrossRef]
27. Belousov, R.I.; Filatov, S.K. Algorithm for calculating the thermal expansion tensor and constructing the thermal expansion diagram for crystals. *Glass Phys. Chem.* **2007**, *33*, 271–275. [CrossRef]
28. Bubnova, R.S.; Firsova, V.A.; Filatov, S.K. Software for Determining the Thermal Expansion Tensor and the Graphic Representation of Its Characteristic Surface (ThetaToTensor-TTT). *Glass Phys. Chem.* **2013**, *39*, 347–350. [CrossRef]
29. Krivovichev, S.V. Topological complexity of crystal structures: Quantitative approach. *Acta Crystallogr.* **2012**, *A68*, 393–398. [CrossRef]
30. Krivovichev, S.V. Structural complexity of minerals: Information storage and processing in the mineral world. *Mineral. Mag.* **2013**, *77*, 275–326. [CrossRef]
31. Krivovichev, S.V. Which inorganic structures are the most complex? *Angew. Chem. Int. Ed.* **2014**, *53*, 654–661. [CrossRef]
32. Krivovichev, S.V. Structural complexity of minerals and mineral parageneses: Information and its evolution in the mineral world. In *Highlights in Mineralogical Crystallography*; Danisi, R., Armbruster, T., Eds.; Walter de Gruyter GmbH: Berlin, Germany, 2015; pp. 31–73. [CrossRef]
33. Krivovichev, S.V. Structural complexity and configurational entropy of crystalline solids. *Acta Crystallogr.* **2016**, *B72*, 274–276. [CrossRef]
34. Blatov, V.A.; Shevchenko, A.P.; Proserpio, D.M. Applied Topological Analysis of Crystal Structures with the Program Package ToposPro. *Cryst. Growth Des.* **2014**, *14*, 3576–3586. [CrossRef]
35. Hughes, J.M.; Brown, M.A. The crystal structure of ziesite, beta-$Cu_2V_2O_7$, a thortveitite-type structure with a non-linear X-O-X inter-tetrahedral bond. *Neues Jahrbuch fur Mineralogie Monatshefte* **1989**, *1*, 41–47.
36. Shannon, R.D.; Calvo, C. Crystal Structure of a New Form of $Cu_3V_2O_8$. *Can. J. Chem.* **1972**, *50*, 3944–3949. [CrossRef]
37. Shannon, R.D.; Calvo, C. Crystal structure of $Cu_5V_2O_{10}$. *Acta Cryst.* **1973**, *B29*, 1338–1345. [CrossRef]
38. Wang, P.; Yang, H.; Wang, D.; Chen, A.; Dai, W.-L.; Zhao, X.; Yang, J.; Wang, X. Activation of Kagome lattice-structured $Cu_3V_2O_7(OH)_2{\cdot}2H_2O$ volborthite via hydrothermal crystallization for boosting visible light-driven water oxidation. *Phys. Chem. Chem. Phys.* **2018**, *20*, 24561–24569. [CrossRef]
39. Filatov, S.K. General concept of increasing crystal symmetry with an increase in temperature. *Crystallogr. Rep.* **2011**, *56*, 953–961. [CrossRef]
40. Goldsmith, J.R. A "simplexity principle" and its relation to "ease" of crystallization. *J. Geol.* **1953**, *61*, 439–451. [CrossRef]